Bending tests on reinforced concrete beams: numerical modelling using a second gradient theory

Gwendal Jouan, Frédéric Collin, Panagiotis Kotronis

VIII International Conference on Fracture Mechanics of Concrete and Concrete Structures
FraMCoS-8
J.G.M. Van Mier, G. Ruiz, C. Andrade, R.C. Yu and X.X. Zhang (Eds)

BENDING TESTS ON REINFORCED CONCRETE BEAMS: NUMERICAL MODELLING USING A SECOND GRADIENT THEORY

G. JOUAN[*†], F. COLLIN[†] AND P. KOTRONIS[*]

[*] LUNAM Université, Ecole Centrale de Nantes, Université de Nantes, CNRS
Institut de Recherche en Génie Civil et Mécanique (GeM)
1 rue de la Noë, F-44321 Nantes, France
e-mail: gwendal.jouan@ec-nantes.fr, panagiotis.kotronis@ec-nantes.fr

[†] Département Argenco – Université de Liège
Institut de mécanique et Génie Civil, Bât. 52
1 Chemin des chevreuils, B-4000 Liège 1, Belgium
e-mail: f.collin@ulg.ac.be

Key words: Second Gradient Theory, Crack, Reinforced Concrete, Damage

Abstract: Being a quasi-brittle material, concrete exhibits a strain softening behavior that cannot be reproduced with classical continuum mechanics models. To regularize the problem, an internal length should be introduced. Several ways to do so have been proposed in the literature. One way is the so called local second gradient model. It is a local theory as it introduces the internal length by enriching the kinematical description of the continuum, adding higher order gradients of the displacement according to the work of Cosserat [1], Toupin [2], Mindlin [3] and Germain [4,5]. The model has been developed by Chambon et al. [6,7] and has this far been used mainly to reproduce the behavior of soils. It is here applied to two bending tests of reinforced concrete beams.

1 INTRODUCTION

Strain localization in quasi-brittle materials, or more generally in materials exhibiting strain softening is a well-known problem [8] [9] [10]. It is a phenomenon that can be clearly observed in experimental tests, and yet cannot be modeled with classical continuum mechanics models. Analytically, the solution is a crack with zero energy dissipation [11]; numerically, it leads to a pathological mesh dependency. These shortcomings are due to the lack of an internal length in the continuum model.

Several ways of introducing an internal length have since been proposed. Non local integral models were first formulated by Pijaudier-Cabot et al. [11] and then extended to damage theory. The gradient models of Aifantis [12] enrich the conventional plasticity and damage theories with gradient of the internal variables. This type of model can be shown to be equivalent to the integral type models. More recently, strain localization due to damage has been treated using the thick level set approach [13].

A rather natural way of introducing (indirectly) a length parameter in a continuum model is to somehow account for the microstructure of the material. The general class of so called microstructured models or higher order continuum models allows for the description of the kinematics of the microstructure by using an additional tensor in the displacement field. Higher order continuum theories can be traced back to the works of the Cosserat brothers [1] and have been generalized and properly formulated by

Germain [4,5] using the method of virtual power.

The local second gradient model developed by Chambon et al. can be seen as a particular case of a higher order continuum and has been used to regularize problems involving localization in geomaterials [6,7]. It is used here to model two different bending tests on reinforced concrete beams. The first one is a 3 point bending test with a beam of 5m span, the second one is a 4 point bending test with a beam of 6.1m span.

2 THE SECOND GRADIENT MODEL AND CONSTITUTIVE LAWS

2.1 Theoretical framework

As detailed in the seminal work of Germain, using the virtual power method one can chose a field of virtual displacement to describe the proper kinematics of the continuum (including its microstructure). The internal stresses, limit conditions and equilibrium equations then appear naturally as long as the linear form representing the virtual power is correctly defined and that it respects the principle of material independence.

Following this, if one chooses the virtual displacement field as the "field of continuous and continuously differentiable velocities", the principle of virtual work yields:

$$\int_D \sigma_{ij} D^*_{ij} + \Sigma_{ijk} u^*_{i,jk} d\Omega - \int_D G_i u^*_i d\Omega - \int_{\partial D} p_i u^*_i + P_i D u^*_i ds = 0 \quad (1)$$

Where u_i is the virtual displacement field, D_{ij} is the symmetric part of its gradient, σ_{ij} is the macro stress (conjugate of first gradient) and Σ_{ijk} is a double stress (conjugate of the second gradient of the velocity field). G_i is the classical body force, p_i is a contact force and P_i a double contact force. Du_i refers to the normal derivative: $Du_i = n_k \partial u_i / \partial x_k$. Here and henceforth * denotes a virtual quantity.

The equilibrium equations and boundary conditions are given by:

$$\frac{\partial \sigma_{ij}}{\partial x_j} - \frac{\partial^2 \Sigma_{ijk}}{\partial x_j \partial x_k} + G_i = 0 \quad (2)$$

$$\sigma_{ij} n_j - n_k n_j D\Sigma_{ijk} - \frac{D\Sigma_{ijk}}{Dx_k} n_j - \frac{D\Sigma_{ijk}}{Dx_j} n_k + \frac{Dn_l}{Dx_l} \Sigma_{ijk} n_j n_k - \frac{Dn_j}{Dx_k} \frac{Dn_l}{Dx_l} \Sigma_{ijk} n_j = p_i \quad (3)$$

$$\Sigma_{ijk} n_j n_k = P_i \quad (4)$$

Where Dq/Dx_j is the tangential derivative.

2.2 Numerical implementation

The second gradient of the displacement in the weak formulation of the problem necessitates the use of C^1 elements in a finite element code. This can be avoided by introducing a new field v_{ij} imposed to be equal to the gradient of u_i by lagrange multipliers [16]. The new weak formulation of the problem then becomes:

$$\int_D \sigma_{ij} D^*_{ij} + \Sigma_{ijk} v^*_{ij,k} d\Omega - \int_D \lambda_{ij} \left(\frac{\partial u^*_i}{\partial x_j} - v^*_{ij} \right) d\Omega - P_e = 0 \quad (5)$$

$$\int_D \lambda^*_{ij} \left(\frac{\partial u_i}{\partial x_j} - v_{ij} \right) d\Omega = 0 \quad (6)$$

The problem is then discretized using 9 nodes finite elements, where 8 of the nodes are used for u_i, 4 for v_{ij} and the center node for λ_{ij}.

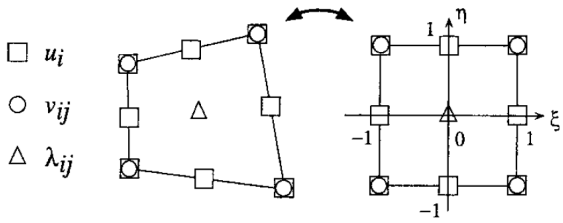

Figure 1: 2nd gradient finite element [7]

This element has been implemented in the finite element code Lagamine and the problem is solved using the classical Newton-Raphson method.

2.3 Constitutive laws

Here we suppose that the model uses two constitutive equations, one linking the macro stress to the first gradient of the displacement and the other linking the double stress to the second gradient of the displacement. The two equations are also supposed to be decoupled. The first gradient law can be any classical constitutive law (involving or not damage, plasticity etc…). The constitutive laws can be written in rate form as:

$$\dot{\sigma}_{ij} = C_{ijkl} \dot{D}^e_{kl} \quad (7)$$

$$\dot{\Sigma}_{ijk} = K_{ijklmn}\dot{u}_{l,mn} \tag{8}$$

If the second gradient law is an isotropic elastic one, the general form of the constitute law involves five material parameters. A particular form of this latter constitutive equation has been proposed by Chambon et al. [7] with a single modulus *B*.

$$\begin{bmatrix}\dot{\Sigma}_{111}\\ \dot{\Sigma}_{112}\\ \dot{\Sigma}_{121}\\ \dot{\Sigma}_{122}\\ \dot{\Sigma}_{211}\\ \dot{\Sigma}_{212}\\ \dot{\Sigma}_{221}\\ \dot{\Sigma}_{222}\end{bmatrix} = \begin{bmatrix} B & 0 & 0 & 0 & 0 & B/2 & B/2 & 0\\ 0 & B/2 & B/2 & 0 & -B/2 & 0 & 0 & B/2\\ 0 & B/2 & B/2 & 0 & -B/2 & 0 & 0 & B/2\\ 0 & 0 & 0 & B & 0 & -B/2 & -B/2 & 0\\ 0 & -B/2 & -B/2 & 0 & B & 0 & 0 & 0\\ B/2 & 0 & 0 & -B/2 & 0 & B/2 & B/2 & 0\\ B/2 & 0 & 0 & -B/2 & 0 & B/2 & B/2 & 0\\ 0 & B/2 & B/2 & 0 & 0 & 0 & 0 & B \end{bmatrix} \begin{bmatrix}\dot{u}_{1,11}\\ \dot{u}_{1,12}\\ \dot{u}_{1,21}\\ \dot{u}_{1,22}\\ \dot{u}_{2,11}\\ \dot{u}_{2,12}\\ \dot{u}_{2,21}\\ \dot{u}_{2,22}\end{bmatrix} \tag{9}$$

The internal length does not appear clearly from these equations. However, analytical solution of localization in a one-dimensional problem with a bilinear first gradient law of moduli A_1 and A_2, exhibits a localized strain band, whose length l_s is given by [14]:

$$tanh\left(\sqrt{\frac{A_1}{B}}(L-l_s)\right) = -\sqrt{\frac{-A_1}{A_2}}tan\left(\sqrt{\frac{-A_2}{B}}l_s\right) \tag{10}$$

It is shown that the internal length l_s is mainly a function of the ratio of B over A_2.

The use of the second gradient model allows for the proper representation of strain localization. It does not however imply uniqueness of the solution. For a one-dimensional tension test or a biaxial compression test, the number of bands and their positions can vary [15]. This is in accordance with experimental results which tend to be poorly reproducible when involving strain localization.

The first gradient law used here for the concrete behavior is the classical Mazars damage law [17]. The equivalent strain is defined as:

$$\varepsilon_{eq} = \sqrt{\langle\varepsilon\rangle_+ : \langle\varepsilon\rangle_+} \tag{11}$$

Where $\langle\ \rangle_+$ denote the positive part and : is the double dot product. The damage is separated in two part D_t and D_c, one due to the tension, and the other due to compression.

$$D_c = 1 - \frac{\varepsilon_{d0}(1-A_c)}{\varepsilon_{eq}} - A_c e^{-B_c(\varepsilon_{eq}-\varepsilon_{d0})} \tag{12}$$

$$D_t = 1 - \frac{\varepsilon_{d0}(1-A_t)}{\varepsilon_{eq}} - A_t e^{-B_t(\varepsilon_{eq}-\varepsilon_{d0})} \tag{13}$$

Where ε_{d0}, A_c, A_t, B_c and A_t are material parameters. The total damage is given by:

$$D = \alpha_t^{\beta} D_t + (1-\alpha_t)^{\beta} D_c \tag{14}$$

α_t is equal to *0* when there is no traction and to *1* when there is no compression. Its value is given by:

$$\alpha_t = \frac{\sum[\langle\varepsilon_i\rangle_+ \varepsilon_{ti}]}{\varepsilon_{eq}^2} \tag{15}$$

ε_{ti} are the principal strains caused by the positive part of the principal stresses.

In the tests modeled here, using Mazars damage law in a two dimensional setting, equation (10) is not valid, but gives nevertheless an indication of the width of the localization zones at their inception.

3 THREE POINT BENDING TEST

3.1 Experimental test

This experimental test was conducted on a reinforced concrete beam according to the specifications of the CEOS.FR benchmark [18]. The beam is of thickness b=200mm, height h=500mm and 5000mm span (see: figure 2). It was subjected to cyclic controlled load.

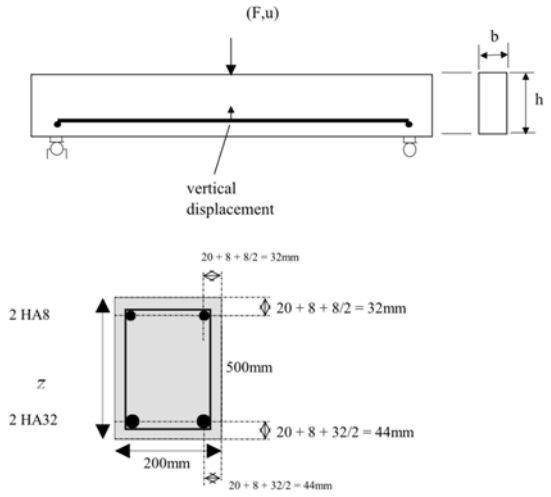

Figure 2: 3 point bending test: beam dimensions [18]

3.2 Numerical model

The bending test is modeled as a two dimensional problem using the 9 node finite element described above. Two meshes have

been used for the simulations. The first mesh consists of 5180 elements, 4148 of which are second gradient elements and 1032 truss elements representing the horizontal reinforcement. The average size of the concrete elements for this mesh is of 0.02mx0.035m. The second mesh consists of 13494 elements with an average size of 0.01mx0.017m for the concrete elements. Concrete and steel elements are supposed to be perfectly bonded. The end nodes at each lower extremities of the beam are blocked vertically; the right node is also blocked horizontally.

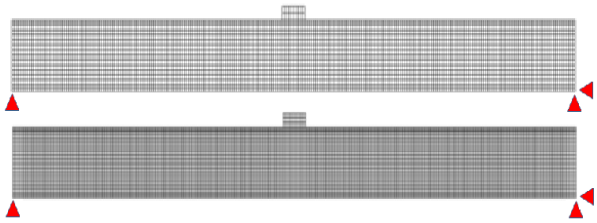

Figure 3: 3 point bending test: finite element meshes

Concrete material parameters for the Mazars damage law are given in table 1:

Table 1: 3 point bending test: concrete material parameters

E (GPa)	ε_{d0}	A_t	B_t	A_c	B_c	β
37.2	9.10^{-5}	0.7	6800	0.42	780	1.1

On the upper part where the loading is applied, and near the supports at both ends of the beam, an elastic linear law is introduced to prevent from unwanted damage. An elasto-plastic law with isotropic hardening is used for the reinforcement.

Table 2: 3 point bending test: reinforcement material parameters

Upper trusses		
E (GPa)	σ (MPa)	Area (cm²)
195	466	16.085 (2HA32)
Lower trusses		
E (GPa)	σ (MPa)	Area (cm²)
195	466	1.0053(2HA8)

The elastic modulus B for the second gradient constitutive law is equal to 1.5.MN.

3.3 Results

Overall, the numerical results are in good accordance with the experimental data. Figure 5 shows the numerical global force versus displacement at the center of the beam compared to the experimental results (note: for the experimental test the beam was loaded and unloaded cyclically whereas in the simulation the beam was loaded with a monotonic increasing displacement).

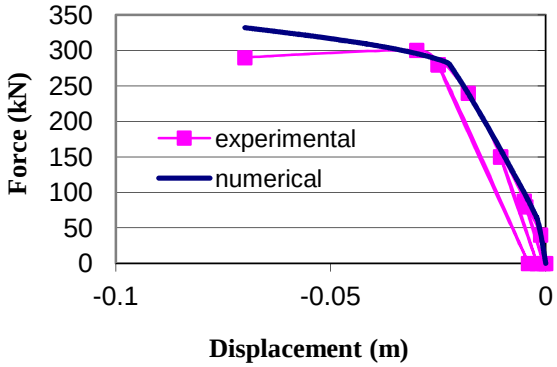

Figure 4: 3 point bending test: force-displacement

The force displacement graph exhibits the classical reinforced concrete behavior in three stages: In the first stage, concrete and steel stay both in the elastic regime; then concrete starts to damage and the slope on the force displacement curve changes. Finally, steel enters in its plastic phase and the second change in the slope appears. The final slope of the numerical simulation doesn't match completely the experimental one. This is due to the second gradient constitutive law which considers no damage (elastic).

Figure 5 shows the pattern of the damage variable in concrete at different stages of loading and for the two mesh sizes.

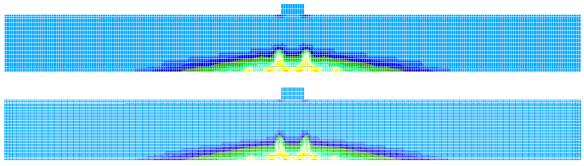

Figure 5.1. 2mm displacement

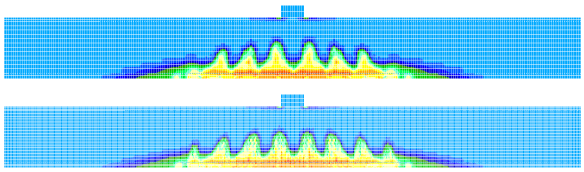

Figure 5.2. 4mm displacement

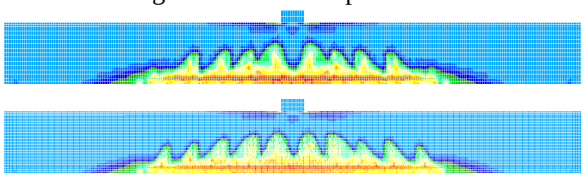

Figure 5.3. 6mm displacement

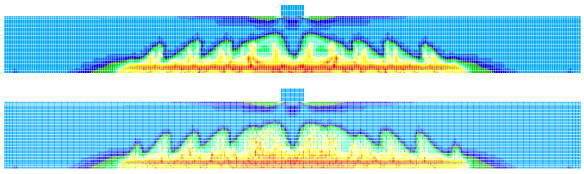

Figure 5.4. 8mm displacement

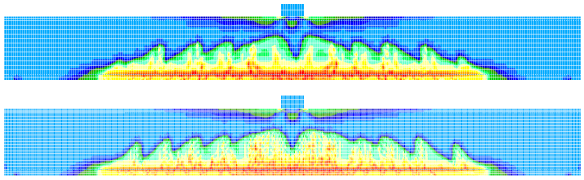

Figure 5.5. 10mm displacement

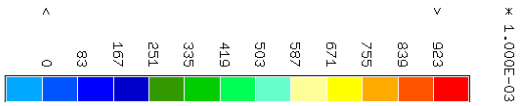

Figure 6.6. Damage scale

Figure 5: 3 point bending test: damage distribution

The damage pattern develops with sudden "peaks" which experimentally correspond to developing cracks. The crack opening is not modeled directly in this simulation as the displacement field remains continuous, but it can be calculated from the damage model either through energetic equivalence or by simply measuring the jump in displacement between two points located on the opposite sides of a damaged zone. This obviously works only when the damaged bands are clearly separated. The width and separation of the damage bands can be controlled by changing the internal length, which in our case would mean changing the slope of either or both the first gradient and second gradient constitutive laws.

The damage distributions for the two different meshes do not match exactly although the global force displacement curves are almost identical. This is due to the fact that, as stated above, the second gradient method doesn't restore the unicity of the solution and small differences can trigger different solutions. All the solutions are still physically acceptable.

For similar bending tests, non-local damage models which define an equivalent strain by averaging over a certain distance l_c, have a tendency to develop damage on the upper compressed part of the beam, even when the local strain is not high enough to cause compressive damage. This is due to the averaging over an area. There is no such problem with this model as all the variables are local.

4 FOUR POINT BENDING TEST

4.1 Experimental test

In this case, the experimental test is a 4 point bending test on a large reinforced concrete beam. (6.10m x 0.8m x 1.6m) (see figure 7, « Mock up », www.ceosfr.org). During the experimental test, the beam was cast and then let to shrink freely. The beam was then fixed to a testing bench with the help of pre-stressed steel bars. The beam is loaded with two rows of pistons up to an imposed force of 2250kN and then unloaded completely.

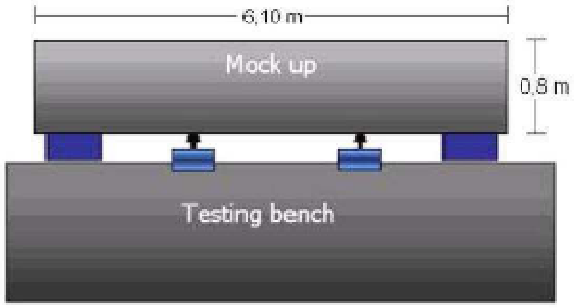

Figure 6: 4 point bending test: experimental test [19]

The reinforcements are indicated in the figure below:

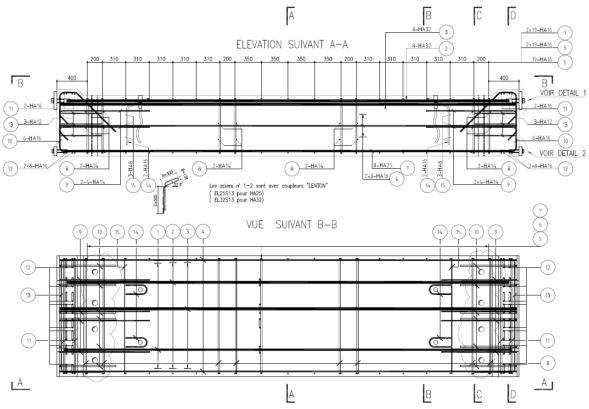

Figure 7: 4 point bending test: reinforcement [19]

The concrete and steel characteristics are given in the following tables:

Table 3: 4 point bending test: concrete characteristics

Category	E (GPa)	ν	f_c (MPa)	f_t (MPa)
C50/60	40.2	0.19	63.7	4.65

Table 4: 4 point bending test: reinforcement characteristics

Catégorie	E (GPa)	f_e (MPa)	ν
Fe500	200	500	0.3

4.2 Numerical model

For this test, it was chosen to model only one half of the beam and to consider a symmetry condition to reduce the computational cost. We used once again the two dimensional 9 nodes second gradient elements to model concrete and one dimensional truss elements for the reinforcement. Two different meshes are used: a coarser one with 5200 elements (4640 second gradient elements and 560 truss elements) and another one with 10000 elements (9209 second gradient elements).

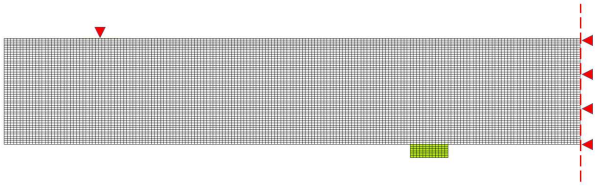

Figure 8: 4 point bending test: numerical model

Material parameters for Mazars damage law are given in table 1. A perfectly elasto-plastic law is considered for the reinforcement.

Table 5: 4 point bending test: concrete material parameters

E (GPa)	ε_{d0}	A_t	B_t	A_c	B_c	β
25.2	$1.1.10^{-4}$	0.7	6800	0.42	780	1.1

The material parameters adopted here don't match exactly the experimental ones. This is because in our calculations only the mechanical loading phase is modeled (the free shrinkage phase that damaged concrete is not simulated). The elastic modulus for the second gradient law B is equal to 1.5.MN.

4.3 Results

The force-vertical displacement curve for the numerical model and the experimental data is given in figure 9. The results for the two different meshes are the same and are in good accordance with the experimental ones (note: only the loading phase is reproduced). During the experiment the beam was unloaded; this is the reason why the global force displacement curve shows only two phases compared to the three phases of the previous test.

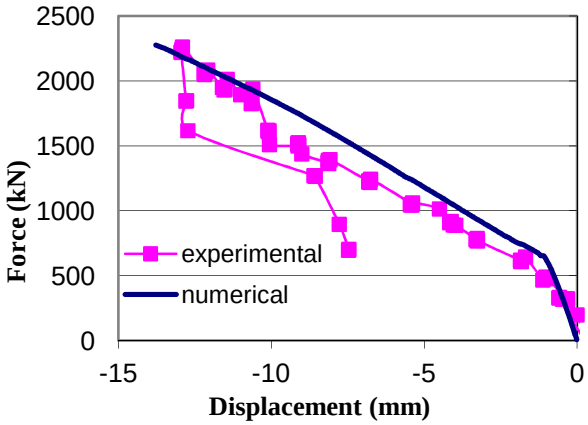

Figure 9: 4 point bending test: force-displacement

Figure 6 presents the pattern of the damage variable in concrete at different stages of loading and for the two mesh sizes.

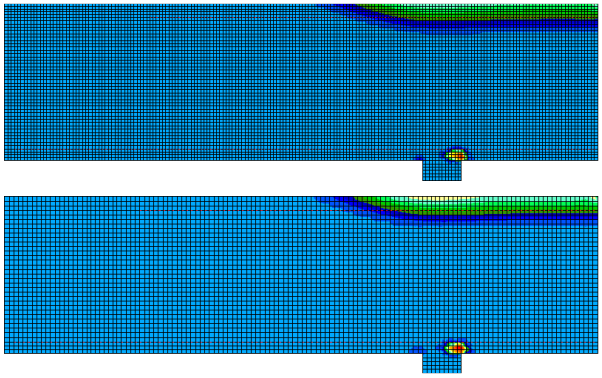

Figure 10.1. F = 940kN

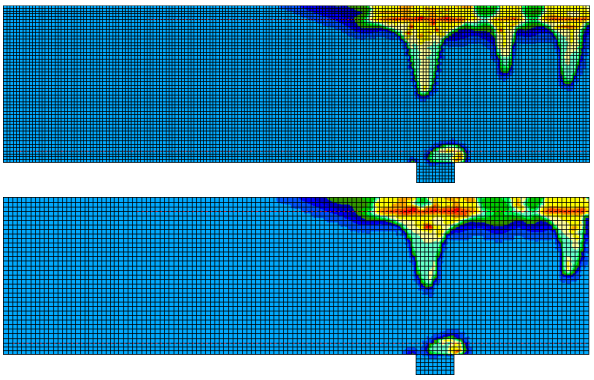

Figure 10.2. F = 1185kN

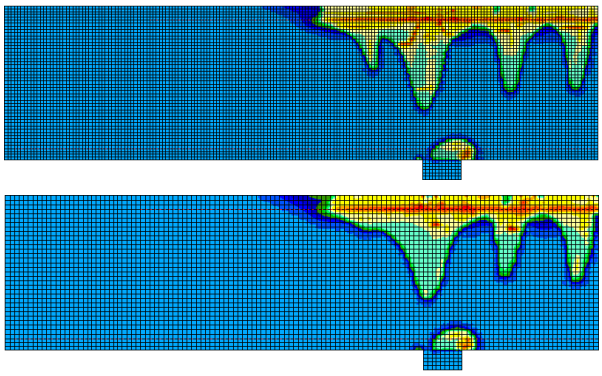

Figure 10.3. F = 1400kN

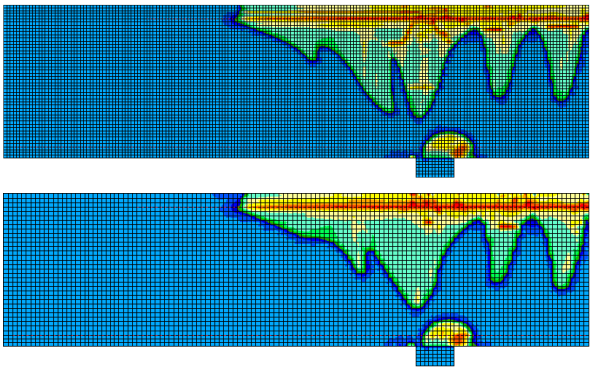

Figure 10.4. F = 1837kN

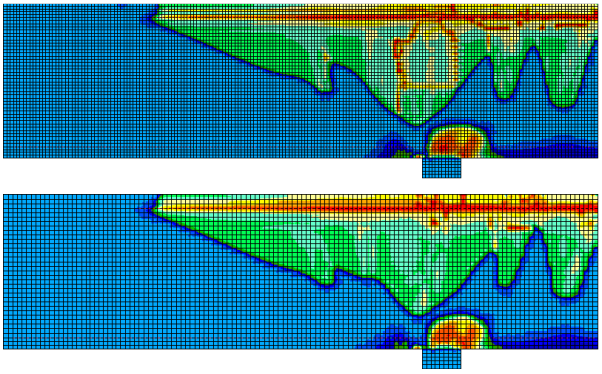

Figure 10.5. F = 2250kN

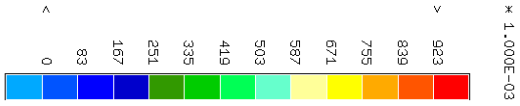

Figure 10.6. Damage scale

Figure 10: 4 point bending test: damage distribution

As was the case with the three point bending test, the damage distributions for the two different meshes do not match exactly, although the global force displacement curves are almost identical.

5 CONCLUSIONS

A second gradient model has been used to model two bending tests of reinforced concrete beams. The results show that the model is able to reproduce the force-displacement curves obtained experimentally. Damage localizes into bands whose width is controlled by the model parameters. The uniqueness of the solution is however not restored. For the two experiments modeled here, the bands are of the same size but their numbers vary (figure 5 and 10). Being a local theory, the second gradient method avoids the limitations caused by the use of a non-local definition of the equivalent strain.

These results are encouraging and represent the first steps toward a wider use of the local second gradient method for concrete structures.

6 ACKNOWLEDGEMENTS

The authors would like to thank the ANR MEFISTO (Maîtrise durable de la fissuration des infrastructures en béton, projet ANR-2008-

Sustainable Cities Program, project number: VD08_323065, 2011) and the Programme National CEOS.fr (www.ceosfr.org) for their financial support.

REFERENCES

[1] Cosserat E., Cosserat F., 2006. Théorie des corps déformables. A. Hermann et Fils.

[2] Toupin R.A., 1962. Elastic materials with couple-stresses. *Archive for rational mechanics and analysis* 11, 385-414.

[3] Mindlin R.D., 1965. Second gradient of strain and surface tension in linear elasticity. *Int. J. Solid and Struct.* 1: 417-438.

[4] Germain P., 1973. La méthode des puissances virtuelles en mécanique des milieux continues: Première partie : théorie du second gradient. *Journal de Mécanique*, 12:235-274.

[5] Germain P., 1973. The method of virtual power in continuum mechanics. Part 2. Microstructure. *J. of Appl. Mathematics*, 25:556-575.

[6] Chambon R., Caillerie D., Matsushima T., 2001. Plastic continuum with micro-structure, local second gradient theories for geomaterials: localization studies. *Int. J. Solid and Struct.* 38:8503-8527.

[7] Matsushima T., Chambon R., Caillerie D., 2000. Second gradient models as a particular case of microstructured models: a large strain finite elements analysis. *Comptes Rendus de l'Académie des Sciences de Paris*, 328 :179–186.

[8] Hill R., Hutchinson J.W., 1975. Bifurcation phenomena in the plane tension test. *J. Mech. Phys. Solids*, 23:239-264.

[9] Rice J.R., 1976. The Localization of plastic deformation. *Theoretical and Applied Mechanics, Proceedings of the 14th International Congress on Theoretical and Applied Mechanics,* 1: 207-220

[10] Rudnicki J.W., Rice J.R., 1975. Conditions for the localization of deformation in pressure-sensitive dilatant materials. *J. Mech. Phys. Solids*, 23:371-394.

[11] Pijaudier-Cabot G., Bažant Z., 1987. Nonlocal damage theory. *J. Engrg Mech.* 113:1512–1533.

[12] Aifantis E., 1984. On the microstructural origin of certain inelastic models. *J. Eng. Mater. Tech*. 106:326-330.

[13] Moës N., Stolz C., Chevaugeon N., 2011. A level set based model for damage growth: The thick level set approach. *Int. J. Numer. Methods in Engrg*, 86:358-380.

[14] Chambon R., Caillerie D., El Hassan N., 1998. One-dimensional localization studied with a second grade model. *European J. Mech. Solids*, 17:637–656.

[15] Bésuelle P., Chambon R., Collin F., 2006. Switching deformation modes in post-localization solutions with a quasibrittle material. *J. Mech. Mater. Struct.* 1:1115–1134.

[16] Matsushima T., Chambon R., Caillerie D., 2002. Large strain finite element analysis of a local second gradient model: application to localization. *Int. J. Numer. Methods in Engrg*, 54:179–186.

[17] Mazars J., 1984. Application de la mécanique de l'endommagement au comportement non linéaire et à la rupture du béton de structure, *Thèse de doctorat d'état de l'Université Paris VI.*

[18] Jason L., 2008. Réponse au benchmark statique monotone du projet national CEOS.FR. Rapport CEA SACLAY, DM2S/SEMT/LM2S, Rapport ANR MEFISTO.

[19] Livrable GT1-4. Prise en compte des résultats expérimentaux dans les modélisations. Programme ANR

MEFISTO (Maîtrise durable de la fissuration des infrastructures en béton). Projet ANR-2008-Sustainable Cities Program, project number: VD08_323065, 2011.